

Spectrum multiplexing of multiwavelength picosecond oscillation of synchronously pumped Raman laser based on a $\text{Sr}(\text{MoO}_4)_{0.8}(\text{WO}_4)_{0.2}$ crystal

© D.P. Tereshchenko,¹ S.N. Smetanin,¹ A.G. Papashvili,¹ K.A. Gubina,² Yu.A. Kochukov,^{1,2} S.A. Solokhin,³ M.N. Ershkov,³ E.V. Shashkov,¹ V.E. Shukshin,¹ L.I. Ivleva,¹ E.E. Dunaeva,¹ I.S. Voronina¹

¹ Prokhorov Institute of General Physics, Russian Academy of Sciences, Moscow, Russia

² National University of Science and Technology MISiS, Moscow, Russia

³ Kovrov State Technological Academy named after V.A. Degtyarev, Kovrov, Russia

e-mail: solokhins@gmail.com

Received December 9, 2022

Revised December 9, 2022

Accepted December 9, 2022

For the first time to our knowledge, a single-phase solid solution $\text{Sr}(\text{MoO}_4)_{0.8}(\text{WO}_4)_{0.2}$ was used as an active medium of a Raman laser. Using the high-intensity synchronous picosecond pumping satisfying the condition of phase capture of the parametric Raman interaction on the second vibrational mode made it possible to oscillate six components of Raman radiation with a combined frequency shift on the first (888 cm^{-1}) and second (327 cm^{-1}) vibrational modes in the wavelength range of 1194–1396 nm. Oscillation efficiency of the multiwavelength Raman laser radiation was as high as 10%. By detuning the Raman laser cavity length, the pulse shortening down to 6 ps for the Raman laser radiation components with the combined frequency shift was obtained, which is an order of magnitude shorter than the pumping pulse duration (64 ps).

Keywords: stimulated Raman scattering, single-phase solid solution, vibrational mode, synchronous pumping.

DOI: 10.21883/TP.2023.04.55936.270-22

Introduction

Currently, noninvasive methods for studying living tissues and organisms based on the action of various physical principles, such as magnetic, electrical or optical interaction of individual particles with matter or field, are of great interest in biotechnology. One of the promising directions in this area is multicolor two-photon microscopy of living tissues [1], which uses ultrashort radiation pulses with high repetition rate at several wavelengths of the near infrared range, which can penetrate into biological tissue to a depth of several centimeters. The radiation wavelengths must be spectrally positioned for resonant excitation of specially designed fluorescent proteins such as mKate2, tdKatushka2, mNeptune, mCardinal, Alexa647 etc., which possess exceptional brightness and photostability, and absorb at different wavelengths positioned in the therapeutic transparency window of biological tissues (1000–1400 nm) [2]. Simultaneous excitation of several „multi-colored“ fluorophores can significantly increase the depth and contrast of fluorescent bioimaging, so it is necessary to use several different lasers, which is not commercially reasonable, or one laser, but with frequency conversion. In Ref. [2], the frequency conversion of a subpicosecond ytterbium fiber laser was carried out through stimulated Raman scattering (SRS) in artificial diamond under synchronous pumping, which was successfully applied to problems of two-photon fluorescence bioimaging. In Ref. [3], an original method was proposed and implemented for shortening the generated radiation

pulses in the course of SRS with a combined frequency shift at several vibrational resonances in SRS-active crystals under synchronous picosecond pumping. Tetragonal crystals with two vibrational resonances: an intense resonance (the first vibrational mode) were used to excite SRS during synchronous picosecond pumping and a spectrally broadened resonance (the second vibrational mode) served to shorten the SRS pulse to its bandwidth-limited duration in the second SRS stage with combined frequency shift. This made it possible to obtain radiation pulses with a duration of 1 ps and less, which are tens of times shorter than the pump pulse [4]. In Ref. [5] it is shown that the use of solid solutions of $\text{Pb}(\text{MoO}_4)_{x-1}(\text{WO}_4)_x$ as an active medium of a synchronously pumped Raman laser can yield an increase in the number of generated components of the SRS radiation.

The present paper is devoted to the study of conditions for increasing the number of generated SRS radiation components with a combined frequency shift. To solve this problem, we used as an active medium of the Raman laser with intense synchronous picosecond pumping a single-phase solid solution $\text{Sr}(\text{MoO}_4)_{0.8}(\text{WO}_4)_{0.2}$ that possesses a higher-intensity second vibrational mode than in a nominally pure SrMoO_4 crystal. This provided the generation of six SRS radiation components with closely-spaced wavelengths, which exceeded the number of generated components in a SrMoO_4 crystal of similar length under similar conditions.

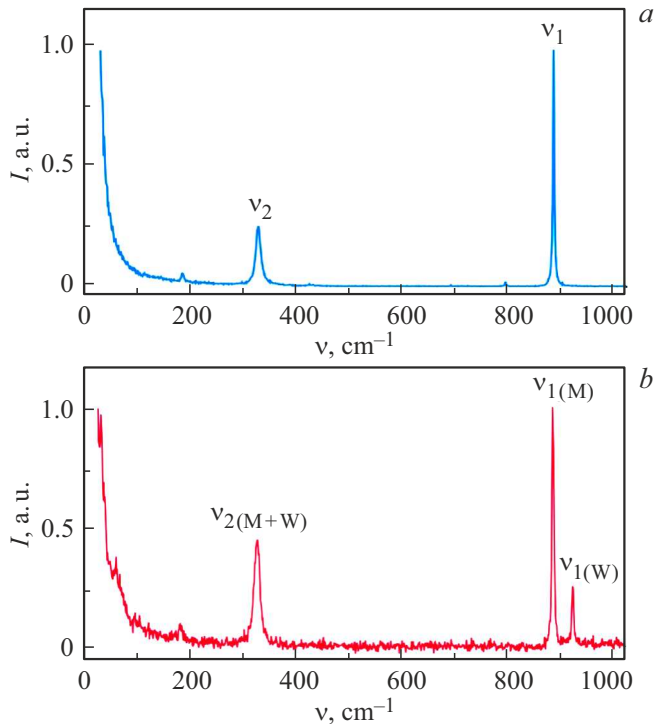


Figure 1. Polarized spectra of Raman scattering of light in the case of polarization of pump and scattered radiation directed along the optical axis of the crystal: *a* — in a SrMoO_4 crystal, *b* — in a $\text{Sr}(\text{MoO}_4)_{0.8}(\text{WO}_4)_{0.2}$ crystal.

1. Characterization of the active crystal

The single crystal of $\text{Sr}(\text{MoO}_4)_{0.8}(\text{WO}_4)_{0.2}$ solid solution was grown from melt by the Czochralski method in the [100] direction using the platinum crucible in air at the Research Center for Laser Materials and Technologies, General Physics Institute of the Russian Academy of Sciences. To prepare the charge, strontium molybdate and tungstate were mixed, obtained by solid-phase synthesis from powders of strontium carbonate SrCO_3 and oxides of tungsten WO_3 and molybdenum MoO_3 , special purity grade (OSCh), in a proportion of 80 and 20 mol.% respectively. To obtain crystals of high optical quality, the volume growth rate was maintained to be no higher than $0.3 \text{ cm}^3/\text{h}$ and the axial temperature gradient in the growth zone was $100^\circ\text{C}/\text{cm}$. The crystals were also post-growth annealed for 6–8 h to prevent their cracking and minimize thermal stresses.

From the resulting $\text{Sr}(\text{MoO}_4)_{0.8}(\text{WO}_4)_{0.2}$ crystal, an active element of length $L = 7 \text{ cm}$ was fabricated with antireflection coatings on plane-parallel end faces. The optical axis of the crystal was oriented perpendicular to the direction of propagation of laser radiation to provide pumping with radiation polarized along the optical axis of the crystal, in order to excite not only the first, but also the second vibrational mode of the crystal [3].

Figure 1 shows the measured polarized spectra of Raman scattering of light in SrMoO_4 and $\text{Sr}(\text{MoO}_4)_{0.8}(\text{WO}_4)_{0.2}$

crystals for the case of pump and scattered radiation polarized along the crystal optical axis.

The first vibrational mode in the $\text{Sr}(\text{MoO}_4)_{0.8}(\text{WO}_4)_{0.2}$ solid solution (Fig. 1, *b*) is a two-frequency mode corresponding to totally symmetric vibrations of the molybdate ($\nu_{1(\text{M})} = 888 \text{ cm}^{-1}$) and tungstate ($\nu_{1(\text{W})} = 921 \text{ cm}^{-1}$) anionic groups. The second vibrational mode ($\nu_2 = 327 \text{ cm}^{-1}$) in the SrMoO_4 crystal (Fig. 1, *a*) has the lowest intensity ($I_1/I_2 = 4.8$, where $I_{1,2}$ are the intensities of the first and second vibrational modes), but it is the broadest ($\Delta\nu_2 = 10.5 \text{ cm}^{-1}$) among scheelite-like crystals [6]. In the $\text{Sr}(\text{MoO}_4)_{0.8}(\text{WO}_4)_{0.2}$ solid solution (Fig. 1, *b*), the intensity of the second vibrational mode ($\nu_{2(\text{M+W})} = 327 \text{ cm}^{-1}$) increases to a value of $I_1/I_2 = 3.2$, comparable to that for nominally pure SrWO_4 . At the same time, its spectral width increases to $\Delta\nu_2 = 12 \text{ cm}^{-1}$ due to the combination of bending vibrations of the molybdate and tungstate anionic groups with close center frequencies [7]. The vibrational resonance linewidth of more than 10 cm^{-1} makes it possible to compress Raman pulses to shorter than 1 ps (up to the reciprocal half-linewidth) [4].

2. Conditions for enriching the spectrum of multiwave SRS radiation with a combined frequency shift

For multiwave SRS with a small spacing between the wavelengths, it is necessary to ensure that not only the first, but also the second vibrational mode participates in the SRS process in the crystal. In the steady-state SRS mode, when the duration of the pump radiation pulses significantly exceeds the dephasing (phase relaxation) time of the crystal oscillations $\tau = (\pi c \Delta\nu)^{-1}$ (where c is the velocity of light in vacuum, $\Delta\nu$ is the vibrational resonance FWHM), the steady-state Raman gain g is proportional to the vibrational line intensity [8]. For example, in a SrMoO_4 crystal pumped with a wavelength of $1.06 \mu\text{m}$, the steady-state Raman gain coefficients for the first and second vibrational modes are $g_1 = 5.6 \text{ cm}/\text{GW}$ [8] and $g_2 \approx g_1 I_2/I_1 = 1.17 \text{ cm}/\text{GW}$, respectively. Therefore, SRS in the first, high-intensity vibrational mode outperforms SRS in the second, lower-intensity vibrational mode.

In an essentially transient SRS regime, the pump pulse duration, on the contrary, is shorter than the dephasing time τ . In this case, the SRS process is determined by the integral cross section of Raman scattering of light, which is proportional to the product of the steady-state SRS gain (g) and the vibrational resonance linewidth ($\Delta\nu$) [8]. Since the second vibrational mode is low-intensity but broadband, its integral cross section can be comparable with that of the first (high-intensity, but narrow-band) vibrational mode, which can provide SRS oscillation not only at the first, but also at the second vibrational mode. So, for the SrMoO_4 crystal we have $g_1 \Delta\nu_1 = 14.6 \text{ GW}^{-1}$ and $g_2 \Delta\nu_2 = 12.3 \text{ GW}^{-1}$. For the $\text{Sr}(\text{MoO}_4)_{0.8}(\text{WO}_4)_{0.2}$ solid solution, the second vibrational line is more intense and broader than in SrMoO_4

(Fig. 1), so the value of $g_2\Delta\nu_2$ even exceeds the value of $g_1\Delta\nu_1$ (by a factor of 1.4), which should provide a more efficient transient SRS at the second vibrational mode.

Another possibility is to use a selective optical resonator in which an SRS-active crystal is installed. With a resonator length equal to 1 m, the round trip time (double pass) of the resonator is more than 6 ns. To ensure the multipass development of Raman oscillation in the resonator, it is necessary that the pumping pulse duration be many times greater than the round trip time of the resonator, since the Raman laser is a laser without population inversion. Such a long-term SRS occurs in a steady-state regime, in which the difference between the coefficients g_1 and g_2 must be compensated by the high Q factor of the resonator for SRS at the second vibrational mode, but usually yields a low efficiency of the SRS conversion with a combined frequency shift [9].

The best choice is to use an optical resonator for non-stationary SRS under the action of ultrashort pumping laser pulses, when the large width of the second vibrational mode becomes important. Since, in this case, the pulse duration is deliberately shorter than the cavity round trip time, the pumping should be implemented by a series of picosecond pulses with a repetition period synchronized with the Raman laser cavity round trip time [10]. The resonator must have a high Q factor for the first Stokes component of the Raman radiation with a high-frequency shift at the first vibrational mode. The output mirror of the resonator must be optimized for efficient multiwave generation of the higher Stokes components of Raman radiation with a combined (high and low frequency) frequency shift in both vibrational modes [3].

In Ref. [11], in such an SrWO₄ crystal Raman laser with synchronous picosecond pumping with the wavelength $\lambda_p = 1063$ nm not only the SRS radiation Stokes components with a high-frequency shift took part in the oscillation (ν_1 , the first one with a wavelength of $\lambda_S = (\lambda_p^{-1} - \nu_1)^{-1} = 1178$ nm and the second with a wavelength of $\lambda_{SS} = [\lambda_p^{-1} - (\nu_1 + \nu_1)]^{-1} = 1322$ nm), but also the second Stokes component with the combined frequency shift ($\nu_1 + \nu_2$) and the wavelength $\lambda_{SS} = [\lambda_p^{-1} - (\nu_1 + \nu_2)]^{-1} = 1227$ nm. In Ref. [6] in a similar SrWO₄ crystal Raman laser the near-threshold generation of the third Stokes component was obtained with an additional lower-frequency shift and a wavelength of $\lambda_{SSS} = [\lambda_p^{-1} - (\nu_1 + \nu_2 + \nu_2)]^{-1} = 1279$ nm, which provided generation of four Stokes components with a small wavelength difference about 48 nm.

In the present paper, we investigate the possibility of enriching the Raman spectrum at many closely spaced wavelengths. In Ref. [6], the significant role of the parametric Raman interaction at the second (low-frequency) vibrational mode (ν_2), which has a relatively small wave mismatch, was also noted

$$\Delta k_2 = (n_S + n_{SSS} - 2n_{SS})2\pi\lambda_{SS}^{-1} + (n_S - n_{SSS})2\pi\nu_2,$$

where n_S , n_{SS} and n_{SSS} are the refractive indices at wavelengths λ_S , λ_{SS} and λ_{SSS} . This wave mismatch is an order of magnitude smaller than for the parametric Raman interaction at the first (high-frequency) vibrational mode. Thus, using the known data on the refractive index of the crystal SrMoO₄ [12], we get $\Delta k_2 = 4.4$ cm⁻¹ (at the second mode) against $\Delta k_1 = 35$ cm⁻¹ (at the first mode).

It is known that there is an effect of phase locking in the parametric Raman interaction, which occurs under the condition [13,14] $I_p > \Delta k/g$, where I_p is the pumping radiation intensity. Thus, for the parametric Raman interaction at the first vibrational mode of the SrMoO₄ crystal ($\Delta k_1 = 35$ cm⁻¹, $g_1 = 5.6$ cm/GW) a very high pumping intensity $I_p > 6.3$ GW/cm² is required. However, for the parametric Raman interaction at the second vibrational mode of the SrMoO₄ crystal ($\Delta k_2 = 4.4$ cm⁻¹, $g_2 = 1.17$ cm/GW), the required pumping intensity is lower, $I_p > 3.7$ GW/cm². Moreover, since our parametric Raman interaction (λ_S , λ_{SS} and λ_{SSS}) occurs at the second SRS cascade, the first Stokes components with the wavelength λ_S plays the role of the pumping wave for this interaction. Then the condition of its phase locking is rewritten in the form $I_S > \Delta k_2/g_2 = 3.7$ GW/cm², where $I_S = I_{out}/(1-R_S)$ is the intensity of the first Stokes component inside the crystal, I_{out} is its intensity at the Raman laser output, R_S is the reflection coefficient of the output mirror of the Raman laser for the first Stokes component. Ignoring the difference in the spatiotemporal structure of the pumping radiation and the first Stokes component, in the best case of high-efficiency SRS we get $I_{out} \approx I_p$. Then the phase locking condition can be written in the form $I_p > (1-R_S)\Delta k_2/g_2$. Therefore, the use of high-Q resonator ($R_S \rightarrow 1$) for the first Stokes component of the SRS radiation facilitates the fulfilment of the phase locking condition of multiwave SRS generation with small difference between wavelengths.

The mathematical modeling of generation of the synchronously pumped SRS SrMoO₄ crystal Raman laser carried out by us confirmed the reduction of generation thresholds of higher Stokes components of the SRS radiation with the combined frequency shift under high-intensity pumping, which satisfies the condition of phase locking in the parametric Raman interaction.

3. Optical scheme of the laser system

The optical scheme of the laser system is shown in Fig. 2.

The radiation from the pumping laser 1 after passing through the Faraday isolator 2 is focused by the concave mirror 3 into the Raman-active element 4, placed in a zigzag optical resonator consisting of two concave mirrors 5 and 6 and two plane mirrors 7 and 8.

A high-power oscillator-amplifier laser system based on YAlO₃:Nd³⁺ crystals with a wavelength of $\lambda_p = 1079$ nm was used as a pump laser. The system operating in the passive mode locking regime generated 440 ns-long trains of pulses with a duration of individual pulses $t_p = 64$ ps

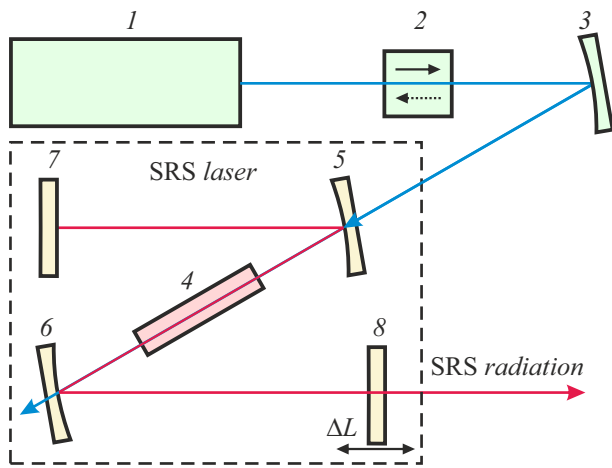


Figure 2. Optical scheme of the laser system: 1 — pump laser; 2 — Faraday isolator; 3 — focusing mirror; 4 — SRS active element; 5–8 — mirrors of the Raman laser resonator

and their repetition period 8 ns. The energy of the laser pulse train was $E_{\text{train}} = 18 \text{ mJ}$, which corresponded to the energy of individual pulses up to $E_p = 320 \mu\text{J}$ [15]. The pumping laser was isolated from the Raman laser by means of a Faraday isolator. The use of a concave mirror 3 with a radius of curvature of 240 cm made it possible to focus the pump radiation beam into a focal spot with the minimum beam radius $r_p = 290 \mu\text{m}$ (at level $1/e^2$) and Gaussian transverse distribution of radiation intensity. This ensured an increase in the intensity of the pump radiation pulses up to $I_p = 2E_p / (t_p \pi r_p^2) = 3.8 \text{ GW/cm}^2$, which satisfies the condition of phase locking of the parametric Raman generation at the second vibrational mode.

The $\text{Sr}(\text{MoO}_4)_{0.8}(\text{WO}_4)_{0.2}$ ($L = 7 \text{ cm}$) crystal described above was used as the active element of the Raman laser. The length of the Raman laser resonator was precisely adjusted (the mirror 8 was installed on a micrometer table, which ensures a precise change in the resonator length ΔL) to synchronize the resonator round trip time with the pump pulse repetition period (8 ns). The end flat mirror 7 was highly reflective at wavelengths of SRS radiation from 1194 to 1396 nm ($R_{1192-1396} > 99\%$). Concave mirrors 5 and 6 (radius of curvature 50 cm) were transparent at the pump wavelength (transmittance $T_{1079} = 97.1\%$) and had the following reflection coefficient distribution over wavelengths of SRS radiation: $R_{1194} = 99.3\%$, $R_{1242} = 99.2\%$, $R_{1294} = 92.9\%$, $R_{1336} = 7.0\%$ and $R_{1396} = 15.3\%$. The output plane mirror 8 had the following distribution of reflection coefficients over Raman wavelengths: $R_{1194} = 99.2\%$, $R_{1242} = 98.5\%$, $R_{1294} = 86.6\%$, $R_{1336} = 24.2\%$ and $R_{1396} = 48.0\%$. The resonator configuration was calculated in the ReZonator software tool [16] to match the size of the fundamental transverse mode of the first Stokes component of the SRS radiation with the pump beam focal radius ($r_p = 290 \mu\text{m}$) at the resonator round trip time, synchronized with the pump pulse repetition period (8 ns).

4. Experimental results

The output Raman radiation was decomposed into a spectrum using a diffraction grating (600 mm^{-1}) and sent to a system of separate recording.

First, the pump synchronization was adjusted with longitudinal displacement of the output mirror 8. Figure 3 shows the output pulse train energy E_{out} as a function of the resonator length detuning ΔL , measured for the first two Stokes components of the SRS radiation (the pump pulse train energy being equal to $E_{\text{train}} = 18 \text{ mJ}$).

It can be seen from Fig. 3 that the width of the detuning line for the first Stokes component is rather large ($\sim 20 \text{ mm}$), while for the second component it is small ($\sim 3 \text{ mm}$). Narrow detuning curves were also observed for other Stokes components with a combined frequency shift. Figure 3 shows on a vertical scale the absolute values of the energy obtained by direct measurements (StarLite Ophir-Spiricon energy meter) after the reflection of SRS radiation from a diffraction grating having a reflection coefficient of about 70% (in the first order of diffraction). Zero on the horizontal scale corresponds to the optimal setting of the synchronous pumping, at which the output characteristics of the laser were studied.

The wavelengths of all generated SRS radiation components were recorded with an OceanOptics HR2000 spectrometer (200–1100 nm, resolution 2 nm) after frequency doubling with a lithium iodate crystal. The radiation linewidths did not exceed the resolution of the spectrometer. Figure 4 shows the result of measurements carried out separately for each component of SRS radiation decomposed into a spectrum by a diffraction grating.

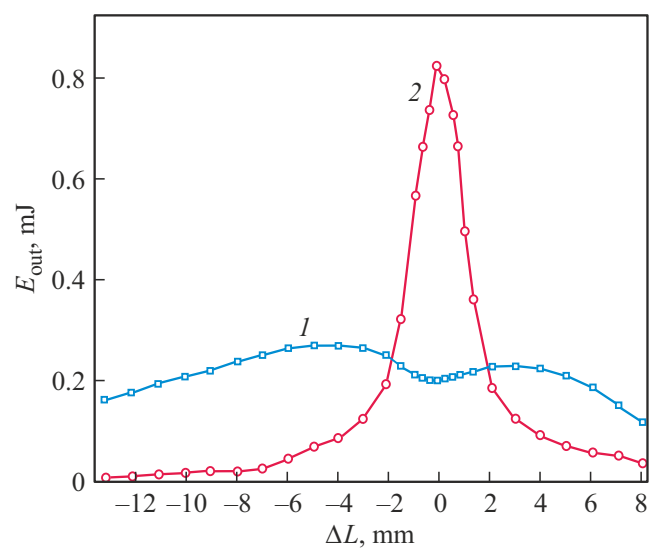


Figure 3. Dependences of the output SRS pulse train energy E_{out} on the resonator length detuning ΔL : 1 — for the first Stokes component with a high-frequency shift; 2 — for the second Stokes component with a combined frequency shift.

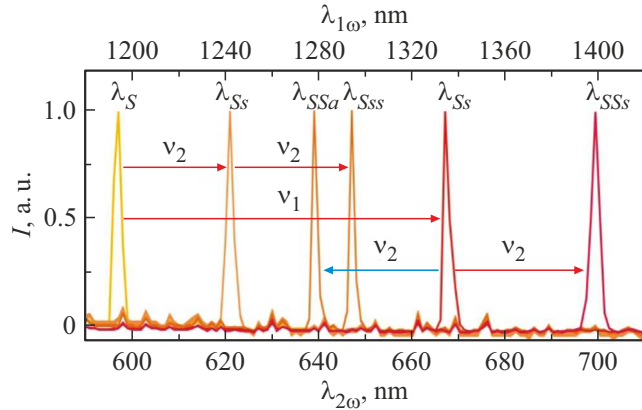


Figure 4. Spectrum of the generated SRS radiation: $\lambda_{2\omega}$ — wavelength of the second harmonic measured by the spectrometer; $\lambda_{1\omega} = 2\lambda_{2\omega}$ — recalculated laser wavelength

The generated radiation components are identified as five Stokes components of SRS radiation

$$\lambda_S = (\lambda_p^{-1} - \nu_1)^{-1} = 1194 \text{ nm},$$

$$\lambda_{SS} = [\lambda_p^{-1} - (\nu_1 + \nu_2)]^{-1} = 1242 \text{ nm},$$

$$\lambda_{SSs} = [\lambda_p^{-1} - (\nu_1 + \nu_2 + \nu_2)]^{-1} = 1294 \text{ nm},$$

$$\lambda_{SS} = [\lambda_p^{-1} - (\nu_1 + \nu_1)]^{-1} = 1336 \text{ nm}$$

and

$$\lambda_{SSs} = [\lambda_p^{-1} - (\nu_1 + \nu_1 + \nu_2)]^{-1} = 1396 \text{ nm},$$

as well as one ant-Stokes component

$$\lambda_{SSa} = [\lambda_p^{-1} - (\nu_1 + \nu_1 - \nu_2)]^{-1} = 1279 \text{ nm}.$$

As a result, generation occurred at six closely spaced wavelengths with an average value of the interval of 40.4 nm between wavelengths. The presence of the Stokes-anti-Stokes component (λ_{SSa}) unambiguously confirms the participation of the parametric Raman interaction at the second vibrational mode.

The output energy was distributed over the SRS radiation components as follows:

- 14% to $\lambda_S = 1194 \text{ nm}$,
- 58% to $\lambda_{SS} = 1242 \text{ nm}$,
- 9% to $\lambda_{SSs} = 1294 \text{ nm}$,
- 10% to $\lambda_{SS} = 1336 \text{ nm}$,
- 6% to $\lambda_{SSs} = 1396 \text{ nm}$ and
- 3% to $\lambda_{SSa} = 1279 \text{ nm}$.

The energy efficiency of the conversion of the pump radiation into the total SRS radiation was 10%.

We also prepared an active element from a nominally pure SrMoO_4 crystal of the same length ($L = 7 \text{ cm}$) with antireflection coatings on plane-parallel end faces. When the $\text{Sr}(\text{MoO}_4)_{0.8}(\text{WO}_4)_{0.2}$ -element was replaced by this

SrMoO_4 -element under the same conditions, generation was also obtained at five Stokes wavelengths ($\lambda_S, \lambda_{SS}, \lambda_{SSs}, \lambda_{SS}$ and λ_{SSs}), but no generation occurred at the Stokes-anti-Stokes wavelength λ_{SSa} , which can be explained by the lower intensity of the second vibrational mode (Fig. 1, a).

Figure 5 shows oscillograms of the four main components of the generated SRS radiation with wavelengths $\lambda_S, \lambda_{SS}, \lambda_{SSs}$, and λ_{SS} (the energy of the pump pulse train being equal to $E_{\text{train}} = 18 \text{ mJ}$). Oscillograms were obtained using four LPD-2A avalanche photodiodes connected to a four-channel Tektronix TDS7404B (4 GHz) oscilloscope.

In Fig. 5, zero on the horizontal scale corresponds to the beginning of the train of pump pulses (not shown in Fig. 5). It can be seen that the pulse trains of the first (curve 1) and second (curve 4) Stokes components with a high-frequency shift begin simultaneously with pumping, i.e., they are generated in the single-pass mode due to high pump intensity (3.8 GW/cm^2).

Pulse trains of Stokes components with a combined frequency shift (curves 2 and 3) had a delay in the devel-

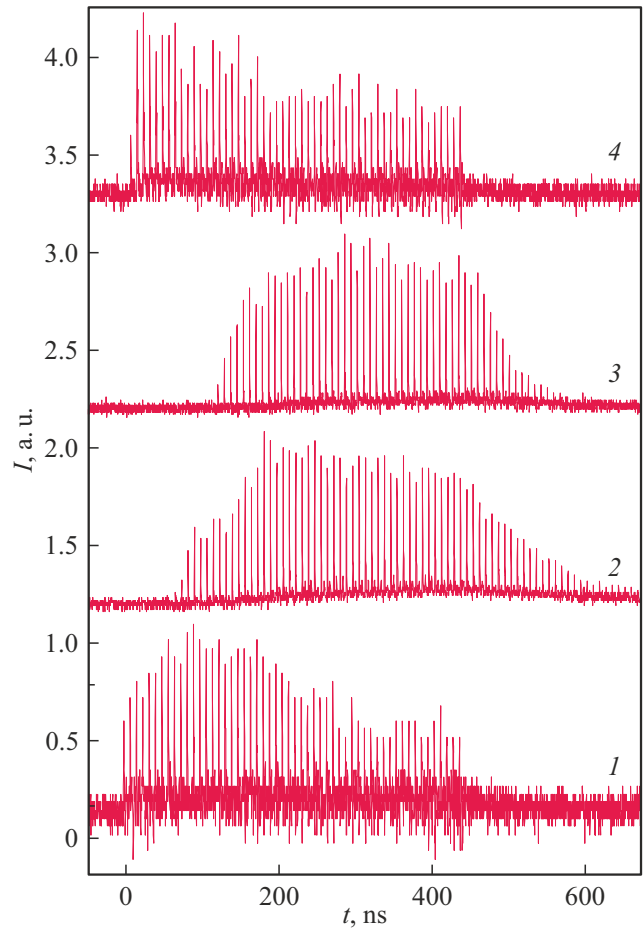


Figure 5. Oscillograms of four components of SRS radiation: 1 — for the first Stokes component (λ_S); 2 — for the second Stokes component with combined frequency shift (λ_{SS}); 3 — for the third Stokes component with combined frequency shift (λ_{SSs}); 4 — for the second Stokes component with a high-frequency shift (λ_{SS}).

opment of parametric Raman generation under the action of intracavity synchronous pumping by the first Stokes component of SRS radiation, locked in a high-Q resonator. The trains of the remaining two components of Raman radiation with a combined frequency shift (λ_{SSa} and λ_{SSs}), which are not shown in Fig. 3, also had a delay. From Fig. 5 it is also seen that the generation of the train of pulses of the component 2 continued for 160 ns after the completion of the train of pulses of the component 1. This is explained by the long lifetime of a photon in a high-Q resonator for the component 2, which is of the order of 100 ns. This is not observed for the component 3, because the resonator has a lower Q factor for it, and the lifetime of a photon in the resonator is an order of magnitude shorter.

Using a streak camera of the PS-1/S1 [17] type (developed by the GPI RAN), the duration of the generated pulses of the output SRS radiation was also measured. Measurements at $\Delta L = 0$ showed that the pulse duration of the Stokes components with a combined frequency shift (λ_{Ss} and λ_{SSs}) was 12 ± 4 ps, and at $\Delta L = 1.5$ mm, corresponding to the half-width of the detuning curve (line 2) in Fig. 3, the pulse duration was shortened to 6 ± 2 ps. For the first (λ_S) and second (λ_{SS}) Stokes components of SRS radiation with a high-frequency shift, no noticeable shortening of the pulses was observed, the pulse duration for them was no less than 20 ps. The shortening of radiation pulses can be explained by the fact that in lasers with synchronous pumping, the pulse duration is determined by the square root of the product of the pump pulse duration and the phase relaxation time of the active medium [18], while the dephasing (phase relaxation) time for the second vibrational mode ($\tau_2 = (\pi c \Delta \nu_2)^{-1} = 0.9$ ps) is much shorter than for the first mode ($\tau_1 = (\pi c \Delta \nu_1)^{-1} = 4$ ps).

Conclusion

For the first time, a single-phase $\text{Sr}(\text{MoO}_4)_{0.8}(\text{WO}_4)_{0.2}$ solid solution was used as the Raman laser medium. The use of high-intensity synchronous picosecond pumping made it possible to obtain the generation of six components of SRS radiation with a combined frequency shift in the first (888 cm^{-1}) and second (327 cm^{-1}) vibrational modes. The number of generated components exceeded that for a nominally pure SrMoO_4 crystal of the same length under the same experimental conditions. The additional generated wave was a Stokes-anti-Stokes component with a combined frequency shift, which unambiguously confirms the participation of the parametric Raman interaction in the second vibrational mode. The enhancement of the generation process consisted in increasing the pumping intensity to fulfill the condition of phase locking for such a parametric Raman interaction in a solid solution, which has a more intense second vibrational mode than in a nominally pure crystal. The generation efficiency of multiwave SRS radiation was 10%. When the resonator length is detuned,

the pulses for the Raman radiation components are shortened with a combined frequency shift to 6 ps, which is an order of magnitude shorter than the pump pulses (64 ps).

Funding

The study was supported by a grant from the Russian Science Foundation № 22-22-20092, <https://rscf.ru/project/22-22-20092/>.

Conflict of interest

The authors declare that they have no conflict of interest.

References

- [1] Ch. Stringari, L. Abdeladim, G. Malkinson, P. Mahou, X. Solinas, I. Lamarre, S. Brizion, J.-B. Galey, W. Supatto, R. Legouis, A.-M. Pena, E. Beaurepaire. *Sci. Rep.*, **7**, 3792 (2017). DOI: 10.1038/s41598-017-03359-8
- [2] E.P. Perillo, J.W. Jarrett, Ye.-L. Liu, A. Hassan, D.C. Ferenec, J.R. Goldak, A. Bonteanu, D.J. Spence, H.-Ch. Yeh, A.K. Dunn. *Light Sci. Appl.*, **6**, e17095 (2017). DOI: 10.1038/lsa.2017.95
- [3] M. Frank, S.N. Smetanin, M. Jelinek, D. Vyhliđal, L.I. Ivleva, P.G. Zverev, V. Kubeček. *Opt. Lett.*, **43** (11), 2527 (2018). DOI: 10.1364/OL.43.002527
- [4] M. Frank, S.N. Smetanin, M. Jelínek, D. Vyhliđal, V.E. Shukshin, P.G. Zverev, V. Kubeček. *Laser Phys. Lett.*, **16** (8), 085401 (2019). DOI: 10.1088/1612-202X/ab2b92
- [5] M. Frank, S.N. Smetanin, M. Jelinek, D. Vyhliđal, M.B. Kosmyna, A.N. Shekhovstov, K.A. Gubina, V.E. Shukshin, P.G. Zverev, V. Kubeček. *Crystals*, **12** (2), 148 (2022). DOI: 10.3390/cryst12020148
- [6] M. Frank, S.N. Smetanin, M. Jelínek, D. Vyhliđal, V.E. Shukshin, L.I. Ivleva, E.E. Dunaeva, I.S. Voronina, P.G. Zverev, V. Kubeček. *Crystals*, **9** (3), 167 (2019). DOI: 10.3390/cryst9030167
- [7] Y. Sun, Zh. Zhu, J. Li, Sh. Gao, H. Xia, Zh. You, Y. Wang, Ch. Tu. *Opt. Mater.*, **49**, 85 (2015). DOI: 10.1016/j.optmat.2015.08.023
- [8] T.T. Basiev, P.G. Zverev, A.Y. Karasik, V.V. Osiko, A.A. Sobol, D.S. Chunaev. *J. Exp. Theor. Phys.*, **99**, 934 (2004). DOI: 10.1134/1.1842874
- [9] P.G. Zverev, T.T. Basiev, A.A. Sobol, I.V. Ermakov, W. Gellerman. In *Advanced Solid-State Lasers*, ed. by C. Marshall. Vol. 50 of OSA Trends in Optics and Photonics (Optica Publishing Group, 2001), paper ME1. DOI: 10.1364/ASSL.2001.ME1
- [10] G.G. Grigoryan, S.B. Sogomonyan. *Sov. J. Quantum Electron.*, **19** (11), 1402 (1989). DOI: 10.1070/QE1989v019n11ABEH009263
- [11] M. Frank, S.N. Smetanin, M. Jelínek, D. Vyhliđal, V.E. Shukshin, L.I. Ivleva, P.G. Zverev, V. Kubeček. *Opt. Laser Technol.*, **119**, 105660 (2019). DOI: 10.1016/j.optlastec.2019.105660
- [12] *Handbook of Optics. Volume IV: Optical Properties of Materials, Nonlinear Optics, Quantum Optics* (The McGraw-Hill Companies, Inc., NY, USA, 2010), 1152 p.
- [13] V.S. Butylkin, G.V. Venkin, L.L. Kulyuk, D.I. Maleev, Yu.G. Khronopulo, M.F. Shalyaev. *Sov. J. Quantum Electron.*, **7** (7), 867 (1977).

- DOI: 10.1070/QE1977v007n07ABEH012668
- [14] L.L. Losev, A.P. Lutsenko. *Sov. J. Quantum Electron.*, **24** (10), 900 (1994). DOI: 10.1070/QE1994v024n10ABEH000206
- [15] D.P. Tereshchenko, E.A. Peganov, S.N. Smetanin, A.G. Papashvili, E.V. Shashkov, L.I. Ivleva, E.E. Dunaeva, I.S. Voronina, M. Frank. *Crystals*, **12**, 495 (2022). DOI: 10.3390/cryst12040495
- [16] Rezonator. [Electronic source] URL: <http://rezonator.orion-project.org> (date of access 02.02.2023)
- [17] N.S. Vorobiev, P.B. Gornostaev, V.I. Lozovoi, A.V. Smirnov, E.V. Shashkov, M.Y. Schelev. *Instrum. Exp. Tech.*, **59** (4), 551 (2016). DOI: 10.1134/S0020441216030246
- [18] V.A. Nekhaenko, S.M. Pershin, A.A. Podshivalov. *Sov. J. Quantum Electron.*, **16** (3), 299 (1986). DOI: 10.1070/QE1986v016n03ABEH005825

Translated by Ego Translating